Subsidiary absorption spin wave instability processes in yttrium iron garnet thin films, critical modes, and the "kink" effect

G. Wiese, P. Kabos,[a] and C. E. Patton
Department of Physics, Colorado State University, Fort Collins, Colorado 80523

(Received 10 December 1992; accepted for publication 15 March 1993)

Butterfly curves of the subsidiary absorption spin wave instability threshold microwave field amplitude versus static field have been measured at 10 GHz on a 12.8-μm-thick single crystal yttrium iron garnet film for two field configurations, one with the static magnetic field in plane and the microwave field out of plane (IP case) and the other with the static field normal to the film plane and the microwave field in plane (PI case). The results for the IP case are similar to earlier results which show a "kink" in the butterfly curve accompanied by a jump of the critical mode wave number k at the kink field. For the PI case, however, there is no observed kink effect. The different butterfly curves for the IP and PI cases are explained on the basis of a new theory for thin films which takes into account the discrete standing wave modes in the film. For the IP case, the theory yields critical modes with wave vectors in the film plane and the kink effect as before. For the PI case, the critical modes have wave vector $\mathbf{k}$ components perpendicular to the film plane, the minimum threshold critical modes are modified significantly, and the theory yields smooth butterfly curves with no kink. Quantitative fits to the data were obtained, based on a single trial function for the $\mathbf{k}$-dependent spin wave linewidth.

I. INTRODUCTION

The parametric excitation of spin waves in ferrite materials can give rise to a broad absorption region somewhat below the ferromagnetic resonance field and a corresponding butterfly curve of the instability threshold microwave field amplitude versus static field.[1] One important effect for single crystal yttrium iron garnet (YIG) spheres and in-plane magnetized films is a distinct kink in the butterfly curve close to the point in field at which the top of the spin wave band at low wave number is at one-half the pump frequency.[2,3] For the sphere case, the kink was explained on the basis of existing first order spin wave instability theory for bulk materials[4] and a $\mathbf{k}$-dependent spin wave relaxation rate which promotes a jump of the critical mode from high to low values of the wave number k at a critical static field.[2]

This work concerns subsidiary absorption butterfly curves for single crystal YIG films with the static magnetic field and saturation magnetization perpendicular to the film plane. In contrast with the situation for in-plane magnetized films, the butterfly curves for the perpendicular case show no kink. The absence of a kink is explained on the basis of the theory which goes beyond the usual continuum plane-wave spin wave approximation and takes into account the discrete standing wave nature of the thin film spin wave modes across the film thickness. For in-plane magnetized films, the discrete nature of the standing modes forces the critical modes to have wave vectors which are in plane as well, and one obtains the same basic kink effect as in spheres. For the perpendicular magnetized film case, however, the critical modes are forced to have wave-vector components perpendicular to the film plane. Here, the discrete nature of the standing modes across the film thickness becomes important and leads to a smooth butterfly curve with no kink effect. The nature of the critical modes is modified significantly.

The experimental results are presented in the next section, Sec. II. The extended theory for first order spin wave instability is described in Sec. III, and connections between the theory and the data are given in Sec. IV.

II. EXPERIMENT AND RESULTS

Subsidiary absorption data were obtained on (111) plane, 12.8-μm-thick YIG films at 9.4 GHz. The films were grown by conventional liquid phase epitaxy techniques on gadolinium gallium garnet substrates. They have narrow ferromagnetic resonance half power linewidths of about 0.5 Oe at 10 GHz. The butterfly curve data were obtained with a modified Varian 4500 microwave spectrometer. A traveling-wave tube (TWT) amplifier was added to the microwave system to obtain the necessary power levels to measure complete butterfly curves. In order to avoid sample heating problems, a microwave pin diode switch was used to control the microwave pulse length and duty cycle. All measurements were made at room temperature. The sample was placed in a TE102 rectangular cavity of moderate $Q=3100$. The cavity was undercoupled and had a reflection coefficient of -9.54 dB at cavity resonance. Rectangular YIG film samples approximately 2×4 mm^2 in size were mounted on a sample holder which allowed for rotation of the sample to place the external magnetic field in plane or perpendicular to the film plane. For the in-plane external field orientation, the microwave magnetic field was oriented perpendicular to the film plane. This configuration will be denoted as the IP configuration. For

[a]On leave from the Slovak Technical University, Bratislava, Czechoslovakia.

 0021-8979/93/74(2)/1218/11/$6.00 © 1993 American Institute of Physics

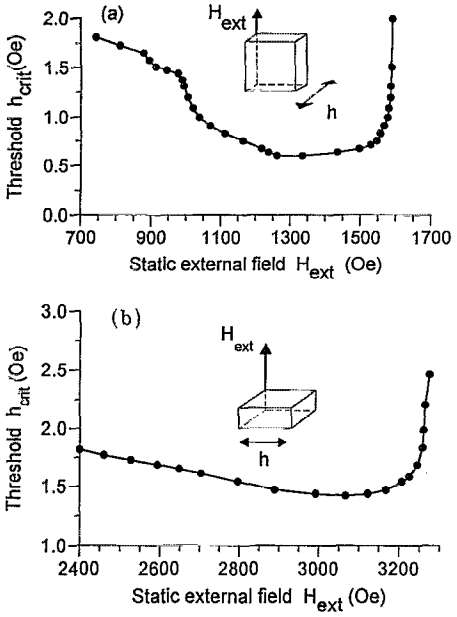

FIG. 1. Experimental subsidiary absorption butterfly curves of the spin wave instability threshold h_{crit} as a function of the static external magnetic field H_{ext} for a 12.8-μm-thick single crystal yttrium iron garnet film and a linearly polarized microwave pump field at 9.4 GHz. (a) Data for the IP configuration with the static field $\mathbf{H}_{ext}$ in plane and the microwave field $\mathbf{h}$ perpendicular to the film plane. (b) Data for the PI configuration with $\mathbf{H}_{ext}$ perpendicular to the film plane and $\mathbf{h}$ in plane.

the perpendicular external field orientation, the microwave field was in the film plane. This configuration will be denoted as the PI configuration.

Butterfly curves of the instability threshold microwave field amplitude h_{crit} as a function of the static field H_{ext} were obtained with the technique of Patton and Jantz.[2] The static field was swept at constant microwave power and the field point for the abrupt increase in absorption which marks the instability threshold was measured. This procedure was repeated for a large number of power levels, and the calibrated data were used to construct the butterfly curves reported below. The calibration to obtain the amplitude of the linearly polarized microwave field at the sample position in the cavity as a function of the microwave power incident on the cavity was obtained from the usual empty cavity approximation and electromagnetic theory. The calibration constant was 5.625 Oe^2/W.

Typical butterfly curves for in-plane static field case (IP configuration) and the perpendicular static field case (PI configuration) are shown in Figs. 1(a) and 1(b), respectively. Each graph gives the threshold microwave field amplitude h_{crit} versus the static external magnetic field H_{ext}. The measured data points are shown by the solid circles. The solid curves show theoretical fits which will be discussed in Sec. IV. The field and pump configurations for each configuration are shown by the figure insets. Note that the microwave field $\mathbf{h}$ is out of plane for the in-plane magnetized film IP configuration and in plane for the perpendicular magnetized film PI configuration. These pumping geometries will be important for the theory and analysis of Secs. III and IV. The kink in the butterfly curve in Fig. 1(a) near $H_{ext} \approx 1000$ Oe for the IP configuration is clearly evident. The butterfly curve in Fig. 1(b) for the PI configuration shows no kink. In this case, the measured threshold curve of h_{crit} versus external field H_{ext} is smooth and without extra structure.

The above experimental results demonstrate the differences in the butterfly curves for in-plane and out-of-plane magnetized films. For the in-plane case, there is a distinct kink effect. In the out-of-plane case, there is no kink at all and the butterfly curve is smooth and undecorated. The origin of the kink, briefly stated above, is related to the $\mathbf{k}$ dependence of the spin wave relaxation rate or the equivalent spin wave linewidth which promotes instability for low k modes. This causes a jump in the critical mode from high k to low k at the point in external field where low k modes become available at one-half the pump frequency. This jump in the critical mode wave number k is the origin of the butterfly curve kink, both for spheres[2] and for in-plane magnetized films.[3] For spheres and in-plane magnetized films, these jumps are allowed because the $\mathbf{k}$ vectors for the critical modes in these cases are more-or-less continuous and not constrained by the sample shape. For the out-of-plane magnetized film case, the critical modes have $\mathbf{k}$ vectors with out-of-plane $\mathbf{k}$ components. These out-of-plane $\mathbf{k}$ components are quantized in units of π/d, where d is the thickness of the film. This constraint on $\mathbf{k}$ modifies the theory, changes the minimum threshold critical modes, and eliminates the kink. The relevant theory and connections to the data shown in Fig. 1 are presented in Secs. III and IV below.

III. THEORY

As indicated above, the origin of the differences in the butterfly curves in Fig. 1 lies in the effect of the thin film and pumping geometry on the critical modes for minimum threshold in the two cases. The theory in Ref. 4 considers spin wave modes in the plane wave approximation. These modes are strictly applicable only for wave numbers which are much larger than π/d, where d is a nominal sample dimension such as the sphere diameter or, in this case, the film thickness. The kink effect described above involves $\mathbf{k}=0$ spin waves. Chen and Patton have addressed the kink problem for spheres by developing an instability for coupled magnetostatic modes.[5] Wiese[6] has developed a general instability theory which analyzes the nonlinear dynamics for the true eigenmodes of an ellipsoidal sample, and successfully applied the theory to the analysis of a fine structure in the threshold curves for single crystal YIG spheres. This theory has now been refined and extended to the specific situation of thin films. This thin film instability theory is able to explain, among other things, the absence of the kink effect for the PI configuration, as shown in Fig. 1(b). A full account of the theory will be published elsewhere.[7] The material below summarizes basic physical considerations and operational equations from the theory. Connections with the experimental results of Sec. II are presented in Sec. IV.

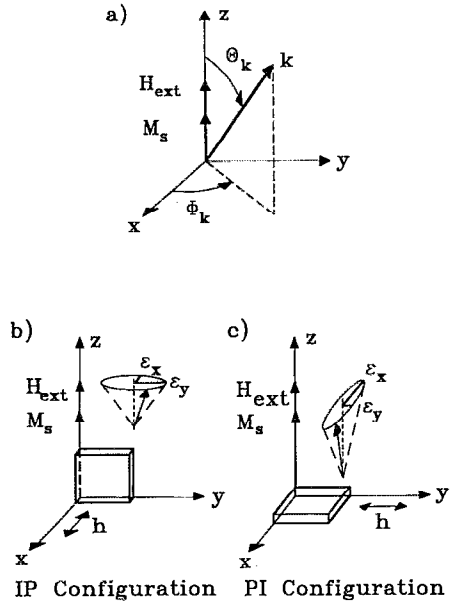

FIG. 2. Coordinate representations for the field, magnetization, and spin wave propagation directions, sample orientations, and pumping configurations: (a) coordinate system for the external magnetic field $\mathbf{H}_{ext}$, static magnetization $\mathbf{M}_s$, and the spin wave wave-vector k with propagation angles θ_k and ϕ_k; (b) coordinate system for the IP configuration with the thin film in the y–z plane, $\mathbf{H}_{ext}$ and $\mathbf{M}_s$ in the z direction, and the microwave field h in the x direction; (c) coordinate system for the PI configuration with the thin film in the x–y plane, $\mathbf{H}_{ext}$ and $\mathbf{M}_s$ in the z direction, and the microwave field h in the y direction. In (b) and (c), schematic elliptical precession cone diagrams for the uniform precession mode in the IP and PI configurations are also shown. In these diagrams, the ϵ_x and ϵ_y parameters denote the relative amplitudes of the x and y components of the uniform precession microwave magnetization responses in the two cases.

The geometry of the problem is shown in Fig. 2. The upper diagram in Fig. 2(a) shows the spin wave wave-vector configuration. The magnetic sample is magnetized to saturation in the z direction. The static field $\mathbf{H}_{ext}$ and the static magnetization vector $\mathbf{M}_s$ lie along the z axis. The spin wave wave-vector k is specified by the wave-number k and the usual polar and azimuthal propagation angles, θ_k and ϕ_k, respectively. The connections with the experimental field and pumping configurations for the in-plane static field IP configuration and the perpendicular static field PI configuration are indicated by the diagrams in the lower part of Fig. 2. For the IP configuration, shown by the diagram in Fig. 2(b) in the lower left part of Fig. 2, the static field is in plane, along the z direction, and the microwave field is out of plane, along the x direction. For the PI configuration, shown by the diagram in Fig. 2(c) in the lower right part of Fig. 2, the static field is out of plane, and the microwave field is in plane and along the y direction. For subsidiary absorption in YIG at x band, both pumping configurations yield elliptically polarized uniform precession modes with the major axes of the precession cones perpendicular to the pump fields, as shown by the x–y precession cone ellipses in the diagrams. The relative lengths of the principal ellipse axes are denoted in terms of ellipticity factors ϵ_x and ϵ_y. These factors will be important in the analysis given below.

A crucial consideration for subsidiary absorption in bulk materials and thin films is in the values of θ_k and ϕ_k for the strongest coupling. This will determine the propagation directions for the modes with the lowest threshold. These minimum threshold modes will be termed the critical modes for instability. In the bulk theory and in the thin film theory, it is found that the coupling is strongest when the polar propagation angle θ_k is approximately $\pi/4$. This result will be evident from the coupling equations given below. The azimuthal propagation angle ϕ_k for the minimum threshold critical modes is related to the spin wave ellipticity. Quantitative considerations are given below. The basic result in the bulk theory is that the coupling is strongest for ϕ_k such that the spin wave elliptical precession cone orientation matches the uniform mode elliptical precession cone orientation. This occurs when the x–y plane projection of the spin wave wave-vector k is perpendicular to the major axis of the uniform mode precession ellipse. With reference to the spin wave wave-vector diagram in Fig. 2(a), this condition is satisfied for the IP configuration in Fig. 2(b) for $\phi_k=0$. Note that, in this case, the major axis of the uniform mode ellipse is along the y axis. For the PI configuration in Fig. 2(c), the matchup occurs for $\phi_k=\pi/2$. In this case, the uniform mode ellipse major axis is along the x axis. The bulk theory, therefore, leads to critical modes with *out-of-plane* k components for both of the cases of interest here.

The critical mode ϕ_k value for thin films may be different from the bulk case value because of the need to impose restrictions on the available k vectors. For thin films, the *out-of-plane* k components are limited to discrete values given by $k_\perp = n\pi/d$, where n is some positive integer. As will be discussed below, the extended instability theory for thin films leads to a *larger* instability threshold field, relative to the bulk theory, for critical modes with a nonzero $k_\perp$. For the IP configuration in Fig. 2(b), this results in a change in the critical mode ϕ_k value from $\phi_k=0$ to $\phi_k=\pi/2$ in order to push $k_\perp$ to zero so that the critical mode k vector is now in plane. The full continuum of k values is then allowed, the bulk theory is again applicable, and one obtains the same basic kink effect as in spheres. This is the result shown in Fig. 1(a).

Due to the geometry of the problem, the situation is different for the PI configuration with the static field perpendicular to the film plane. It is clear from Figs. 2(a) and 2(c) that for a given θ_k value in the $\pi/4$ range, $k_\perp$ will always be approximately equal to $k/2^{1/2}$. *No rotation* in ϕ_k can serve to reduce $k_\perp$ to zero. In this case, therefore, one must include the effect of the true thin film standing modes with $k_\perp = n\pi/d$ on the critical modes and the resulting microwave threshold field amplitude. As will be shown in Sec. IV, these considerations lead to (1) no kink effect and (2) a smooth butterfly curve for the perpendicular static field PI configuration. It is significant that the extended theory can be used to fit quantitatively the butterfly curve data for both configurations with the *same* choice of relax-

ation rate or spin wave linewidth parameters. These fits will be discussed in detail in Sec. IV.

The analytic theory follows the basic formalism of Suhl,[1] Schlömann,[8] and Patton,[4] modified appropriately to deal with the true eigenmodes of the sample.[6] For the thin film case, these eigenmodes are the usual spin wave modes modified appropriately to account for the discrete values of $k_\perp$ discussed above. The basic results are summarized below. The full theoretical development is given in Ref. 7. The summary uses the basic notation established in Refs. 6 and 7.

Consider the set of standing spin wave amplitudes b_k which are parametrically pumped by a linearly polarized microwave magnetic field of amplitude h and frequency ω_p applied perpendicular to the static field and saturation magnetization direction. The parametric excitation of the standing spin wave modes at the half pumping frequency $\omega_p/2$ can be described by an equation of the form

$$\dot{b}_k = -[\eta_k + i(\omega_k - \omega_p/2)]b_k + \sum_{k'} c_{kk'} h b^*_{k'}, \tag{1}$$

where b_k is a complex spin wave amplitude, η_k is a phenomenological relaxation rate, and ω_k is the frequency of the b_k mode. The $c_{kk'}$ coefficient describes the coupling between the microwave pump field h and the $(b_k, b_{k'})$ standing modes. It is important to emphasize that Eq. (1) applies to *standing modes*, that is, to modes composed of the superposition of *two* modes with wave vectors of $+\mathbf{k}$ and $-\mathbf{k}$. Specific expressions for these $c_{kk'}$ coefficients from the bulk theory and the extended theory for thin films will be given shortly. The relaxation rate η_k is often given in linewidth units by means of a spin wave linewidth parameter $\Delta H_k = 2\eta_k/\gamma$, where γ is the gyromagnetic ratio for the material, taken as positive. For YIG, γ is equal to 1.76×10^{-7} $\mathrm{Oe}^{-1}\,\mathrm{s}^{-1}$ or $2\pi \cdot 2.8$ GHz/kOe. It is important to note that the relaxation parameters ΔH_k and η_k are $\mathbf{k}$ dependent. The use of appropriate trial functions for $\Delta H_k(\mathbf{k})$ are crucial to obtain good fits between theory and data for butterfly curves in single crystal YIG.[2,8,9] Such a trial function for $\Delta H_k(\mathbf{k})$, based on Ref. 2, will play an important role in the fits of the theory to the data presented in Sec. IV.

Equation (1) is the basic equation which leads to expressions for the spin wave instability threshold microwave field amplitude h_{crit} for particular sets of spin waves at wave-vector $\mathbf{k}$ and frequency $\omega_k = \omega_p/2$. Based on explicit expressions for the $c_{kk'}$, one solves Eq. (1) for the time dependent $b_k(t)$. For the microwave field amplitude h below some threshold value, h_c, the $b_k(t)$ decay to zero. When h exceeds h_c, the $b_k(t)$ diverge. One then determines the *minimum* such threshold field based on the available spin wave modes for a given static field H_{ext}. From the $(\omega_k - \omega_p/2)$ term in Eq. (1), the minimum threshold modes are generally limited to frequencies near $\omega_k = \omega_p/2$. This minimum threshold will be denoted as h_{crit}. These theoretical h_{crit} values correspond to the measured h_{crit} values shown in Fig. 1. The above procedure is tedious and usually requires numerical methods. In the bulk theory, the $c_{kk'}$ coefficients are diagonal. That is, the $c_{kk'}$ are nonzero only when $k = k'$ is satisfied. In this limit, it is possible to use a much simpler procedure to determine thresholds. One simply sets $\dot{b}_k(t)$ in Eq. (1) to zero, solves the resulting equation for h_c, and then determine the minimum threshold as indicated above. This is the basic approach used in Refs. 4 and 6–10, and, where applicable, the approach to be used here.

First, consider the results for first order instability in the bulk sample or thick film limit. As discussed here, the $c_{kk'}$ coefficients are diagonal in this case. The bulk theory $c_{kk'}$ are given by

$$c^{\mathrm{bulk}}_{kk} = (\cos\phi_k \rho^x_k + i \sin\phi_k \rho^y_k)\delta_{kk'}, \tag{2}$$

where the ρ^x_k and ρ^y_k factors reflect the variation in coupling with the azimuthal spin wave angle ϕ_k. These factors are obtained as

$$\rho^x_k = \tfrac{1}{4}\gamma\omega_m \sin\theta_k \cos\theta_k (\epsilon_x + \epsilon_y\epsilon_k)/\epsilon_k \tag{3}$$

and

$$\rho^y_k = \tfrac{1}{4}\gamma\omega_m \sin\theta_k \cos\theta_k (\epsilon_y + \epsilon_x\epsilon_k)/\epsilon_k. \tag{4}$$

In Eqs. (3) and (4), $\omega_m = \gamma 4\pi M_s$ denotes the saturation induction $4\pi M_s$ in frequency units, and the ϵ_x, ϵ_y, and ϵ_k parameters are ellipticity factors. These ellipticity factors play a key role in the quantitative theory and will be considered in detail shortly.

It is important to note the θ_k dependence of the coupling coefficients in Eqs. (3) and (4). From the $\sin\theta_k \cos\theta_k$ factor in both equations, it is clear that the coupling between the microwave pump field h and the $(b_k, b_{k'})$ modes is strongest for a polar spin wave propagation angle θ_k near $\pi/4$. A small effect on the θ_k value for maximum coupling occurs due to the θ_k dependence of ϵ_k in the ellipticity terms in Eqs. (3) and (4), but the basic point for emphasis here is that, where possible, the minimum threshold critical modes will have longitudinal $\mathbf{k}$ components, along the z axis in the diagrams of Fig. 2, *and* transverse $\mathbf{k}$ components, in the x–y plane, which are roughly equal. This $\pi/4$ positioning of the $\mathbf{k}$ vector for the minimum threshold critical modes is important for bulk samples and will be especially important for thin films. The diagram in Fig. 2(a) deliberately reflects this positioning.

Turn now to the ϕ_k preferences for the minimum threshold critical modes which are implied by Eqs. (1)–(4). The relative magnitudes of the ρ^x_k and ρ^y_k factors determine the ϕ_k preference. If ρ^x_k is greater than ρ^y_k, the minimum threshold critical modes will have $\phi_k = 0$. If ρ^y_k is greater than ρ^x_k, then the critical mode azimuthal angle will flip to $\phi_k = \pi/2$. This is the same ϕ_k-flip effect first discussed in Ref. 4. It is important to note that these ϕ_k preferences are directly tied to the ellipticity matchup considerations discussed above. It is the matchup between the spin wave ellipticity and the uniform precession cone projections shown in Fig. 2 that determines the ϕ_k preferences given above.

The ellipticity factors given in Eqs. (3) and (4) play a crucial role in the theory. The ϵ_x and ϵ_y factors, and an ϵ_0 factor defined below, apply to the polarization of uniform mode discussed above and denoted schematically in Fig. 2.

These factors describe the complex uniform precession response to an applied microwave pump field $h\cdot\cos(\omega_p t)$, taken as the real part of $h\cdot\exp(-i\omega_p t)$, where h is the amplitude of the microwave pumping field defined above. The x–y plane complex microwave magnetization response for the uniform precession mode, $\mathbf{m}(t)$, is given by

$$\mathbf{m}(t)=4\pi M_s(\epsilon_x\mathbf{x}+\epsilon_y\mathbf{y})\cdot h e^{-i\omega_p t}, \tag{5}$$

where $\mathbf{x}$ and $\mathbf{y}$ represent unit vectors along the positive x and y axes for the diagrams in Fig. 2. The ϵ_x and ϵ_y terms reflect the lengths of the principal ellipse axes for the uniform mode precession cones in Figs. 2(b) and 2(c). These factors may be written in analytic form in terms of Larmor and antiLarmor terms in the uniform mode off-resonance response, $X_L=1/(\omega_p-\omega_0)$ and $X_A=1/(\omega_p+\omega_0)$, respectively. For the in-plane static field IP configuration, ϵ_x and ϵ_y are given by

$$\epsilon_x^{\parallel}=(X_L-X_A)/\epsilon_0 \tag{6}$$

and

$$\epsilon_y^{\parallel}=(X_L+X_A), \tag{7}$$

with

$$\epsilon_0=\omega_U/\omega_H. \tag{8}$$

In the above, ω_U denotes the uniform mode or ferromagnetic resonance (FMR) frequency given by the Kittel equation and $\omega_H=\gamma H_{\text{int}}$ denotes a static internal field frequency parameter. For the IP configuration, with the static field in plane, the static internal field H_{int} is equal to the static external field H_{ext}. For the PI configuration, with the static field perpendicular to the film plane, one has the condition $H_{\text{int}}=H_{\text{ext}}-4\pi M_s$. The corresponding ϵ_x and ϵ_y factors for the perpendicular static field PI configuration are given by

$$\epsilon_x^{\perp}=-i(X_L+X_A) \tag{9}$$

and

$$\epsilon_y^{\perp}=-i(X_L-X_A). \tag{10}$$

Note also that the above factors correspond to the ellipse orientations given in the lower diagrams in Fig. 2. The precession ellipse major axis for the IP configuration in Fig. 2(b) is in plane and along the y axis. The precession ellipse major axis for the PU configuration in Fig. 2(c) is along the x axis.

The ϵ_k ellipticity factor in Eq. (2) is for the spin waves at frequency ω_k. This spin wave ellipticity factor is given by

$$\epsilon_k=\omega_k/[\gamma(H_{\text{int}}+Dk^2)], \tag{11}$$

where D is the material spin wave stiffness constant, typically 5.4×10^{-9} for YIG. Recall that the minimum threshold spin waves are at $\omega_k=\omega_p/2$. This condition, in combination with the spin wave dispersion relation,

$$\omega_k=\gamma[(H_{\text{int}}+Dk^2)(H_{\text{int}}+Dk^2+\omega_m\sin^2\theta_k)], \tag{12}$$

yields a specific and simple connection between the spin wave mode wave-number k and polar propagation angle θ_k. This means that the spin wave ellipticity factor ϵ_k can be viewed as a θ_k-dependent function $\epsilon_k(\theta_k)$. The θ_k dependence of ϵ_k is relatively weak, however, and serves only to shift the minimum threshold critical mode wave vector to θ_k values slightly smaller than $\pi/4$. Note that the condition $\epsilon_k(\theta_k)\geqslant 1$ is always satisfied.

The ϵ_x, ϵ_y, and ϵ_k factors given above can be used to verify $\phi_k=0$ preference for the IP configuration and the $\phi_k=\pi/2$ preference for the PI configuration. For subsidiary absorption, the static field is always well below the field for FMR. In this situation, the Larmor and antiLarmor X_L and X_A terms are both positive and $X_L>X_A$ is satisfied. As noted above, the spin wave ellipticity factor ϵ_k always satisfies $\epsilon_k>1$. For the IP configuration, $H_{\text{int}}=H_{\text{ext}}$ and $\omega_H<\omega_U$ are also true. Based on the above connections for the IP configuration, one obtains the condition $\epsilon_y>\epsilon_x$ and finally the relation $\rho_k^x>\rho_k^y$. This corresponds to the $\phi_k=0$ preference discussed above. In the PI configuration, one obtains $\rho_k^y>\rho_k^x$, corresponding to a $\phi_k=\pi/2$ preference.

Return now to the instability threshold field. For bulk samples or thick films, one obtains the spin wave instability threshold field amplitude $h_{\text{crit}}^{\text{bulk}}$ from Eq. (1) with $\dot{b}_k(t)$ set to zero and $c_{kk'}$ taken as diagonal and specified by c_{kk}^{bulk} in Eq. (2). The result can be written as

$$h_{\text{crit}}^{\text{bulk}}=\text{Min}(\eta_k/|c_{kk}^{\text{bulk}}|)\big|_{\omega_k=\omega_p/2}. \tag{13}$$

The "Min" specification in Eq. (8) indicates that the entire $(\eta_k/|c_{kk}^{\text{bulk}}|)$expression must be minimized with respect to the available spin wave $\mathbf{k}$ values and subject to the condition $\omega_k=\omega_p/2$. Equation (11) is equivalent to the results in Ref. 4 for bulk ellipsoidal samples. From the θ_k dependence of the c_{kk}^{bulk} coupling coefficient given through the θ_k dependent terms in Eqs. (3) and (4), it is clear that the minimization selects critical spin wave modes with θ_k approximately equal to $\pi/4$. The $\phi_k=0$ preference applicable to the IP configuration and the $\phi_k=\pi/2$ preference applicable to the PI configuration have been discussed above. Specific threshold field formulas from the bulk theory for these configurations are given below as $h_{\text{crit}}^{\text{bulk-}\parallel}$ and $h_{\text{crit}}^{\text{bulk-}\perp}$, respectively

$$h_{\text{crit}}^{\text{bulk-}\parallel}=\text{Min}(\eta_k/|\rho_k^{x-\parallel}|)\big|_{\omega_k=\omega_p/2}, \tag{14}$$

$$h_{\text{crit}}^{\text{bulk-}\perp}=\text{Min}(\eta_k/|\rho_k^{y-\perp}|)\big|_{\omega_k=\omega_p/2}. \tag{15}$$

Note that the ρ_k^x and ρ_k^y terms in Eqs. (14) and (15) have additional "$\parallel$" and "$\perp$" superscripts to specifically indicate the applicable ϵ_x and ϵ_y ellipticity factors from Eqs. (6)–(10). These ellipticity factors are different for the IP and PI configurations.

As mentioned above, in doing the minimization to determine h_{crit}, it is also necessary to include a $\mathbf{k}$-dependent spin wave relaxation rate η_k or spin wave linewidth ΔH_k. The bulk theory formulas given in Eqs. (14) and (15), in combination with this $\mathbf{k}$-dependent spin wave linewidth, yield the same basic kink effect as in spheres. The data in Ref. 3 and in Sec. II show that a kink effect is seen for the parallel case but not for the perpendicular case. The dif-

ference lies in the effect of the thin film sample geometry and the static field configuration on the minimum threshold critical modes.

The qualitative aspects of the theory differences for thin films were briefly introduced above. There are three basic quantitative changes from the bulk theory. First, the nonzero $c_{k'k}$ coefficients are no longer purely diagonal. There are *off-diagonal* $c_{kk'}$ elements for which the perpendicular components of $\mathbf{k}$ and $\mathbf{k}'$, to be denoted by $k_\perp$ and $k'_\perp$, respectively, differ by π/d. Second, these off-diagonal elements in $c_{kk'}$ are *smaller* than their bulk theory counterparts by a factor of $2/\pi$. Third, the $c_{kk'}$ formulas *differ in form* for the IP and PI configurations under consideration here.

The thin film theory yields the following $c_{kk'}$ coupling coefficients for the IP and PI configurations:

$$c^{\parallel}_{kk'}=\left(\frac{2}{\pi}\cos\phi_k\rho_k^{x-\parallel}\,\delta_{k'_\perp,k_\perp\pm\pi/d}+i\sin\phi_k\rho_k^{y-\parallel}\,\delta_{k'_\perp,k_\perp}\right)\delta_{k'_\parallel,k_\parallel}, \tag{16}$$

$$c^{\perp}_{kk'}=\frac{2}{\pi}(\cos\phi_k\rho_k^{x-\perp}+i\sin\phi_k\rho_k^{y-\perp})\times\delta_{k'_\perp,k_\perp\pm\pi/d}\delta_{k'_\parallel,k_\parallel}. \tag{17}$$

The notation is the same as used for the bulk theory equations. As before, the ρ_k^x and ρ_k^y terms in Eqs. (16) and (17) have additional $\parallel$ and $\perp$ superscripts to specifically indicate the applicable ϵ_x and ϵ_y ellipticity factors from Eqs. (6)–(10). The key differences here from the bulk theory and Eq. (2) are in the $2/\pi$ multipliers and the $\delta_{k',k_\perp\pm\pi/d}$ factors which render the $\cos\phi_k\rho_k^{x-\parallel}$ element in Eq. (16) and the entire coefficient in Eq. (17) nondiagonal. The $c_{kk'}$ coefficients have elements which now couple *pairs* of standing spin wave modes with $k_\perp$ values which *differ* by π/d. The $2/\pi$ factors always appear with these $\delta_{k'_\perp,k_\perp\pm\pi/d}$ delta function terms. For the IP configuration and Eq. (16), only the first element, the $\cos\phi_k\rho_k^{x-\parallel}$ or $\phi_k=0$ preference term is affected. For the PI configuration and Eq. (17), the entire coefficient is affected. These differences from the diagonal $c_{kk'}$ in the bulk theory and the specific differences between the $c_{kk'}$ coefficients given above for the IP and PI configurations lead to the preservation of the kink effect for the in-plane static field IP configuration, as in spheres, and the disappearance of the effect for the PI configuration.

The new features in the theory for thin films are contained in the $2/\pi$ coupling factor for terms involving critical modes with a nonzero $k_\perp$ and in the coupling of pairs of spin wave modes differing in $k_\perp$ by π/d. Similar features have been observed by Rezende and Azevedo in connection with a general first order instability theory for parallelopiped shaped samples.[11]

The solutions to Eq. (1) with $c_{kk'}$ coefficients as given in Eq. (16) or (17) are complicated and best accomplished by numerical methods. The nondiagonal nature of the $\cos\phi_k\rho_k^x$ term in Eq. (16) and the entire $c_{kk'}$ coefficient in

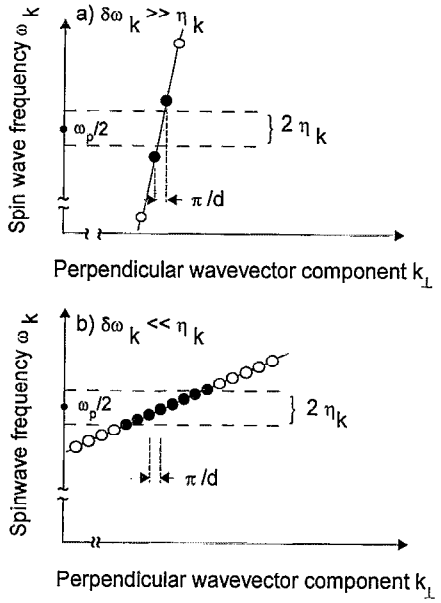

FIG. 3. Schematic representations of the two limiting cases for the spin wave mode frequency separation $\delta\omega_k$ relative to the spin wave relaxation frequency η_k. Both graphs show spin wave frequency ω_k as a function of the perpendicular out-of-plane component of the spin wave wave vector, $k_\perp$, for a thin film of thickness d. The mode separation in $k_\perp$ is π/d. The mode spacing in ω_k is $\delta\omega_k$. Horizontal dashed lines on both graphs indicate frequency bands of width $2\eta_k$ centered at the nominal critical mode spin wave frequency of $\omega_p/2$, or half the pump frequency. Graph (a) is for the case $\delta\omega_k\gg\eta_k$. Graph (b) is for the case $\delta\omega_k\ll\eta_k$. The open and solid circles both denote the discrete spin wave modes vs static external field H_{ext} for the thin film of thickness d. The modes designated by solid circles are the modes which are strongly coupled to the microwave pump field in subsidiary absorption.

Eq. (17), with *coupled* modes separated in $k_\perp$ by π/d, makes it necessary to examine *complete coupled mode solutions* rather than *single* $b_k(t)$ *behaviors*. It is useful to examine two limiting cases before discussing specific solutions for the critical modes and instability threshold microwave field amplitude results for the two static field configurations. The point of distinction between these two cases is the frequency separation of the pair modes separated in $k_\perp$ by π/d, relative to the spin wave relaxation rate η_k. This difference will be specified by $\delta\omega_k=\partial\omega_k/\partial k_\perp\cdot\pi/d$. In the first case, case A, the condition $\delta\omega_k\gg\eta_k$ is satisfied. The limit would be valid for *nonzero* $\partial\omega_k/\partial k_\perp$ and thin films, for example. In the second case, case B, the condition $\delta\omega_k\ll\eta_k$ is satisfied. This limit would apply to (i) very thick films or (ii) situations for which $\partial\omega_k/\partial k_\perp$ is zero. The thick film limit, case (B)(i), corresponds essentially to bulk materials. Here, one expects that the thin film theory would reduce to the bulk formulas discussed above. The $\partial\omega_k/\partial k_\perp=0$ condition, case B(ii), represents a specific connection between the wave-number k and spin wave polar angle θ_k for spin waves at frequency $\omega_k=\omega_p/2$. For case B(ii), the basic equations for threshold fields from the bulk theory would apply, but with the Min condition replaced by the condition $\partial\omega_k/\partial k_\perp=0$.

The two limiting case A and case B situations are indicated schematically in Fig. 3. Both diagrams in Fig. 3

show the spin wave frequency ω_k for sequences of coupled mode pairs versus the perpendicular wave-vector component $k_\perp$. The individual modes are shown by the solid and open circles. The coupled modes have $k_\perp$ values which are spaced π/d apart and frequency values which are $\delta\omega_k$ apart. The lines of mode circles are positioned in frequency in a symmetric fashion relative to the half pump frequency, $\omega_p/2$. The diagrams also have two horizontal dashed lines which show a frequency band of width $2\eta_k$ and centered at $\omega_p/2$. Figure 3(a) is for the case A limit, $\delta\omega_k \gg \eta_k$. For this situation, the mode separation in frequency is *much greater* than the frequency width $2\eta_k$. The mode circles closest to $\omega_p/2$ are both *outside* the $2\eta_k$ band. The numerical solutions of Eq. (1) for both configurations in this thin film limit show that the two modes closest to $\omega_p/2$, indicated by the solid circles, are the modes which are most strongly coupled to the microwave field and which dominate the instability process.

Figure 3(b) is for the case B limit, $\delta\omega_k \ll \eta_k$. The layout of the diagram in Fig. 3(b) is the same as in Fig. 3(a), but with the $2\eta_k$ band shown on an expanded scale. In this $\delta\omega_k \ll \eta_k$ limit, the circles which represent the individual modes are more closely spaced in frequency than before. As a result, there are *many* modes inside the $2\eta_k$ band. It is important to note at this point that the relaxation rate η_k represents a physical frequency broadening for individual modes. This means that the mode circles within the $2\eta_k$ band really have no separate identity as individual distinct modes. Because of this η_k broadening, the diagram in Fig. 3(b) corresponds to a coupling to a *single* broadened mode at frequency $\omega_k = \omega_p/2$. All of the modes within the band are collectively coupled to the microwave pumping field at ω_p. Hence, all of the modes within $2\eta_k$ band in Fig. 3(b) are shown by solid circles. This is more or less the same as the bulk situation. From the discussion above, however, the case B limit, $\delta\omega_k \ll \eta_k$, is possible under two conditions, (1) very thick films and (2) thin films and special values of the frequency ω_k and wave-vector **k** for which the condition $\partial\omega_k/\partial k_\perp = 0$ is satisfied. These conditions have been specified as case B(i) and case B(ii), respectively.

The discussion above shows that the coupled mode scheme can be quite different for thin films, thick films, or under the condition $\partial\omega_k/\partial k_\perp = 0$. First, consider the application of these two limiting cases to the in-plane static field IP configuration. For case A, with the critical mode pair well outside the $2\eta_k$ band, one can obtain a simple analytical result for the spin wave instability minimum threshold field amplitude, $h_{\text{crit}}^{\parallel\,(A)}$. In order to demonstrate clearly the differences between the bulk theory and the thin film theory for the IP configuration, the general equation for $h_{\text{crit}}^{\parallel\,(A)}$ is developed in two steps. In the first step, one obtains

$$h_{\text{crit}}^{\parallel\,(A)} = \text{Min}\left[\left(\eta_k \Big/ \left|\frac{2}{\pi}\cos\phi_k \rho_k^{x-\parallel}\right|\right); \left(\left|\frac{\eta_k}{\sin\phi_k \rho_k^{y-\parallel}}\right|\right)\right]. \tag{18}$$

The right-hand side of Eq. (18) contains $\phi_k = 0$ and $\phi_k = \pi/2$ preference terms which are similar to the corresponding terms in the bulk theory. The difference from the bulk theory is twofold. First, the terms involving $\cos\phi_k \rho_k^x$ and $\sin\phi_k \rho_k^y$ now occur separately rather than in terms of a single coupling coefficient as in Eq. (2). Second, the coupling term corresponding to a $\phi_k = 0$ preference, the $\cos\phi_k \rho_k^{x-\parallel}$ term, is now multiplied by an *additional* $2/\pi$ factor. These differences change significantly the ϕ_k preference for the minimum threshold critical modes in the IP configuration thin film case.

Recall that in the bulk theory applied to the IP configuration, the condition $\rho_k^{x-\parallel} > \rho_k^{y-\parallel}$ leads to a $\phi_k = 0$ preference for the minimum threshold critical modes. For YIG films and a nominal pump frequency of 10 GHz, the $2/\pi$ reduction in coupling for this $\phi_k = 0$ preference term is sufficient to change the ϕ_k preference for the minimum threshold critical modes to $\pi/2$. As a result, the minimum threshold critical mode **k** vector is now flipped in plane and the applicable term in Eq. (18) becomes the $\sin\phi_k \rho_k^{y-\parallel}$ term. Under these conditions, the thin film case A spin wave instability threshold amplitude for the IP configuration is given by

$$h_{\text{crit}}^{\parallel\,(A)} = \text{Min}(\eta_k/|\rho_k^{y-\parallel}|)\big|_{\omega_k=\omega_p/2}. \tag{19}$$

Equation (19) has the same form as Eq. (14) for the bulk theory, except that $\rho_k^{x-\parallel}$ is replaced by $\rho_k^{y-\parallel}$. In this thin film case A limit for the in-plane static field IP configuration, therefore, one *still* expects to obtain a kink effect. There are differences from the bulk result, however, in that (1) the critical modes now have *in-plane* **k** vectors with $\phi_k = \pi/2$ and (2) the $\rho_k^{y-\parallel}$ function rather than the $\rho_k^{x-\parallel}$ function must be used for specific butterfly curve calculations and fits. Specific butterfly curve fits will be discussed in Sec. IV.

Turn now to case B for the in-plane static field IP configuration. For case B(i), corresponding to $\delta\omega_k \ll \eta_k$ in the thick film limit, the $c_{kk'}$ coupling coefficients reduce to the diagonal expressions in Eqs. (2)–(4), with ellipticity factors $\epsilon_x^{\parallel}$ and $\epsilon_y^{\parallel}$ corresponding to the static in-plane field configuration of Fig. 2(b) and the bulk h_{crit} formula given in Eq. (14) applies without modification. Case B(ii) is not applicable to thin films in the IP configuration. For the IP configuration with $\phi_k = 0$, corresponding to nonzero $k_\perp$, the relations $k^2 = k_\parallel^2 + k_\perp^2$ and $\sin^2\theta_k = k_\perp^2/(k_\parallel^2 + k_\perp^2)$ are satisfied. From Eq. (12), this leads to a spin wave frequency ω_k which is always an *increasing* function of $k_\perp$. The condition $\partial\omega_k/\partial k_\perp = 0$ cannot be satisfied.

Consider now the critical modes and spin wave instability threshold field amplitudes for the perpendicular static field PI configuration, based on the $c_{kk'}$ coupling coefficient given by Eq. (17). As for the PI configuration, simple analytical solutions are possible for the case A and case B limits discussed above. In the case A limit, for the condition $\delta\omega_k \gg \eta_k$, one obtains an expression for the spin wave instability threshold field amplitude $h_{\text{crit}}^{\perp\,(A)}$ given by

$$h_{\text{crit}}^{\perp\,(A)} = (\pi/2)\cdot\text{Min}(\eta_k/|\cos\phi_k \rho_k^{x-\perp} + i\sin\phi_k \rho_k^{y-\perp}|)\big|_{\omega_k=\omega_p/2}. \tag{20}$$

As for the IP configuration, one minimizes an expression of the form $(\eta_k/|c_{kk}^{\text{eff}}|)$, where c_{kk}^{eff} represents an effective

diagonal-like coupling coefficient. In contrast with the situation for the IP configuration, however, the c_{kk}^{eff} is now *identical* with the coupling coefficient in the bulk theory. The only difference between Eq. (20) for $h_{\text{crit}}^{\perp\,(\text{A})}$ and the bulk theory threshold is in the additional $\pi/2$ factor. Recall that in the bulk theory for the PI configuration, the condition $\rho_k^{y-\perp} > \rho_k^{x-\perp}$ leads to a $\phi_k = \pi/2$ preference. The same condition and preference apply here. The threshold $h_{\text{crit}}^{\perp\,(\text{A})}$, therefore, can be written as

$$h_{\text{crit}}^{\perp\,(\text{A})} = (\pi/2) \cdot \text{Min}(\eta_k/|\rho_k^{y-\perp}|)\big|_{\omega_k=\omega_p/2}$$
$$= (\pi/2) h_{\text{crit}}^{\text{bulk}-\perp} . \tag{21}$$

Based on the above case A result, one would expect to observe a kink effect for subsidiary absorption in perpendicular magnetized thin films. One would also expect to observe thresholds which are larger by a factor of $\pi/2$ than for thick films.

It is necessary, however, to consider also the case B situation for the PI configuration in thin films. Recall that case B corresponds to a situation for which the frequencies of the coupled modes are close together, relative to the relaxation rate η_k, as shown schematically in Fig. 3(b). For case B(i), the bulk limit, one would obtain the bulk threshold, or $h_{\text{crit}}^{\text{bulk}-\perp}$. This, however, is not applicable to the thin film situation. Case B(ii) is applicable to the thin film situation. For the PI configuration, moreover, one can satisfy the case B(ii) condition, $\partial\omega_k/\partial k_\perp = 0$, for particular values of the wave vector **k** or, equivalently, particular values of the wave number k and polar spin wave propagation angle θ_k. Note that for the PI configuration, the connection between $k_\perp$, $k_\parallel$, and $\sin^2\theta_k$ is now given by $\sin^2\theta_k = k_\parallel^2/(k_\parallel^2 + k_\perp^2)$. From Eq. (12), one can see that the spin wave frequency ω_k has a minimum with respect to $k_\perp$. One may evaluate the $\partial\omega_k/\partial k_\perp = 0$ condition analytically and obtain

$$(1+\epsilon_k^2) Dk^2 = 4\pi M_s \sin^2\theta_k . \tag{22}$$

Recall that for case B, the bulk theory analytic expressions are applicable without modification. However, rather than using the Min minimization procedure to determine the lowest threshold critical mode among the available spin wave states at $\omega_k = \omega_p/2$, one simply uses the condition $\partial_k/\partial k_\perp = 0$ as specified in Eq. (22). The critical mode in this case is specified by the spin wave dispersion equation, Eq. (12), with $\omega_k = \omega_p/2$ and the additional (k,θ_k) connection from Eq. (22). Note that the critical mode for the PI configuration has $\phi_k = \pi/2$. The threshold $h_{\text{crit}}^{\perp\,(\text{B})}$ is given by

$$h_{\text{crit}}^{\perp\,(\text{B})} = (\eta_k/|\rho_k^{y-\perp}|)\big|_{\omega_k=\omega_p/2,\partial\omega_k/\partial k_\perp=0} . \tag{23}$$

Equation (23) involves no minimization procedure, insofar as the critical mode frequency $\omega_k = \omega_p/2$, the mode wave-number k, and the mode propagation angles θ_k and ϕ_k are already completely specified. Hence, butterfly curves based on $h_{\text{crit}}^{\perp\,(\text{B})}$ analyses will *show no kink effect.*

The question of a kink effect for perpendicular magnetized films reduces, therefore, to a consideration of the case A and case B threshold microwave field expressions given by Eq. (21) for $h_{\text{crit}}^{\perp\,(\text{A})}$ and Eq. (23) for $h_{\text{crit}}^{\perp\,(\text{B})}$. The *observed* threshold h_{crit} for a given value of the applied static field H_{ext} will correspond to the lowest of the two thresholds. The case A $h_{\text{crit}}^{\perp\,(\text{A})}$threshold gives a kink effect. The case B $h_{\text{crit}}^{\perp\,(\text{B})}$ threshold gives no kink. Because of the minimization procedure, the case A threshold, $h_{\text{crit}}^{\perp\,(\text{A})}$, would *always* be the lowest possible value if the $\pi/2$ multiplier in Eq. (21) was not present. This multiplier, however, forces an overall increase in the kink-related threshold. For YIG films at x band, these considerations make the $h_{\text{crit}}^{\perp\,(\text{B})}$ threshold the lowest value over most of the butterfly curve field range. Only at the extreme high field part of the butterfly curve does the case A threshold prevail. This result will be evident from the numerical analyses presented in the next section.

IV. ANALYSIS AND DISCUSSION

The butterfly curve data presented in Sec. II for the IP and PI configurations, and as shown in Fig. 1, have been used as a basis for theoretical fits, following the theoretical development summarized in Sec. III. Fits were made for the three different theoretical h_{crit} expressions developed in Sec. III. For the in-plane static field IP configuration, the case A $h_{\text{crit}}^{\parallel\,(\text{A})}$ threshold expression from Eq. (19) was used. For the perpendicular static field PI configuration, the case A $h_{\text{crit}}^{\perp\,(\text{A})}$ threshold expression from Eq. (21) and the case B $h_{\text{crit}}^{\perp\,(\text{B})}$threshold expression from Eq. (23) were used. The fitting procedure for all three expressions was the same as described in detail in Ref. 2.

Following Ref. 2 and as discussed above in connection with the kink effect, the use of a suitable **k**-dependent spin wave linewidth $\Delta H_k(\mathbf{k})$ trial function is critical in obtaining successful fits of the theory to the data. The fits obtained here for both the IP and the PI configurations were made with the same $\Delta H_k(\mathbf{k})$ function used in Ref. 2

$$\Delta H_k(\mathbf{k}) = A_0 + A_1 \sin^2(2\theta_k) + B_1 L(k/k_c) . \tag{24}$$

The constant A_0 term in Eq. (24) represents all **k**-independent relaxation processes which contribute to the spin wave relaxation. Such processes include certain Kasuya–LeCraw losses, fast and slow impurity relaxation mechanisms, and **k**-independent three magnon relaxation terms. The $B_1 L(k/k_c)$ and the $A_1 \sin^2(2\theta_k)$ terms in Eq. (24) represent specific aspects of a **k**-dependent $\Delta H_k(\mathbf{k})$ which were first derived by Sparks[12] for the three magnon confluence relaxation process in YIG under various approximations. The L function is given by

$$L(x) = \frac{1}{1.39x} \ln\left(1 + \frac{8x^2(1+2x^2)}{(1+8x^2)}\right) . \tag{25}$$

The function $L(k/k_c)$ is reasonably linear in k for $k \ll 0.1\ k_c$ or so, peaks at $k \approx 1/2k_c$, and trails off slowly for $k \gg k_c$. As discussed in Ref. 2, $L(k/k_c)$is essentially a steplike function in k with the step effect at $k \approx 0$. This steplike k dependence for $\Delta H_k(\mathbf{k})$ is critical to the kink effect reported and explained in Ref. 2. Although it has nothing to

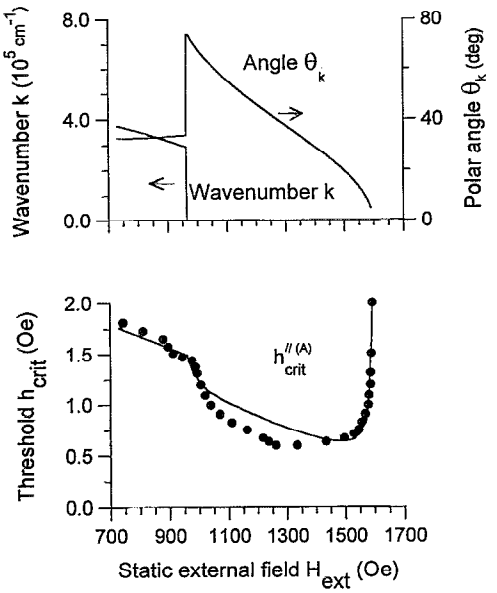

FIG. 4. Butterfly curve data from Fig. 1(a) and a theoretical fit to the data for the IP configuration, as discussed in text, with companion plots of the corresponding theoretical critical mode spin wave wave number k and polar propagation angle θ_k parameters vs static external field H_{ext}.

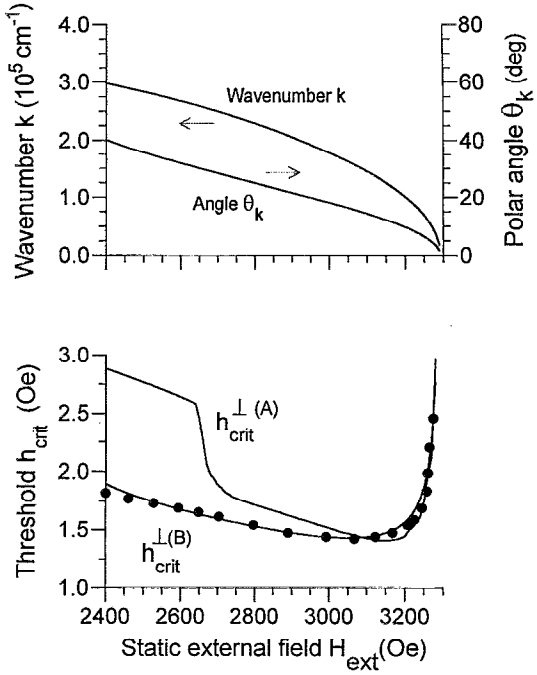

FIG. 5. Butterfly curve data from Fig. 1(b), along with theoretical case A and case B butterfly curves for the PI configuration, based on the fitting parameters for the curve in Fig. 4 and as discussed in text. The companion plots show the theoretical critical mode spin wave wave number k and polar propagation angle θ_k parameters vs static external field H_{ext} for the case B butterfly curve.

do with the kink effect *per se*, the $A_1 \sin^2(2\theta_k)$ term in Eq. (24) is critical to the butterfly curve fits in general above the minimum threshold field position.[2,13]

Even though these k-dependent terms have some basis in theory, the *form* of Eq. (24) with the three explicit additive terms is justified mainly on the basis of the butterfly curve fits which could be uniquely obtained in Ref. 2 and the follow-up empirical verification of the predicted critical mode behavior in Ref. 3. There is no theory at the present time for a general k-dependent spin wave linewidth. The remarkable result from Ref. 2 is that Eq. (24) provides a very good quantitative fit to a rather complicated butterfly curve and also provides a consistent explanation for the kink effect. The corresponding jump in the critical mode k value from high to low values at the kink field, discussed in the Introduction, implies a jump in θ_k from about 30°–40° to 80°–85° or so. These jumps have been verified experimentally.[3]

First, consider again the subsidiary absorption data for the IP configuration shown in Fig. 1(a). Recall that for this case, the static field is in the film plane and the microwave field is out of plane. The subsidiary absorption butterfly curve in Fig. 1 clearly shows the kink effect. The applicable case A $h^{\parallel(A)}_{crit}$ threshold expression from Eq. (19) in Sec. III, in conjunction with the operational relation for $\Delta H_k(\mathbf{k})$ in Eq. (24), was used to obtain a "best fit" theoretical butterfly curve to the data. The experimental butterfly curve from Fig. 1(a) along with the results of this fit are shown in Fig. 4. The fitting parameters for the curve in Fig. 1 are $A_0 = B_1 = 0.19$ Oe, $A_1 = 0.215$ Oe, and $k_c = 10^6$ cm^{-1}. These parameter values are close to the values cited for the single crystal YIG sphere ΔH_k parameters of Ref. 2, except for k_c. The present best fit k_c value, however, is quite close to Sparks theoretical value of 8.5×10^5 cm^{-1} cited in Ref. 2.

The lower part of Fig. 4 shows the theoretical butterfly curve fit to the data for the IP case. The upper part of Fig. 4 shows the k and θ_k values for the corresponding theoretical minimum threshold critical modes as a function of static field. The butterfly curve fit is quite good and the kink effect is nicely reproduced. As already discussed, the critical mode shows a jump from relatively high k values to $k=0$ at the kink field, with a corresponding upward jump in θ_k from 35° to 75° or so. These results nicely match the butterfly curve and Brillouin light scattering results of Ref. 3 as well.

Consider now the PI configuration with the static field and magnetization perpendicular to the film plane and the microwave field in plane. The experimental butterfly curve for this case was shown in Fig. 1(b) and is shown again in the lower part of Fig. 5. This butterfly curve shows no kink effect. For this configuration, as discussed in Sec. III, it is necessary to consider two different theoretical curves. First, one needs to use the case A $h^{\perp(A)}_{crit}$ threshold expression from Eq. (21) in Sec. III, and determine the minimum threshold and the corresponding critical mode as a function of the static field. Second, one needs to utilize the case B $h^{\perp(B)}_{crit}$ threshold expression from Eq. (23) in Sec. III, and evaluate the threshold and critical mode k and θ_k values subject to the additional constraint on the dispersion specified by $\partial\omega_k/\partial k_\perp = 0$, for which Eq. (23) is valid. Such curves have been calculated for the *same* ΔH_k parameters

used for the IP configuration fits shown in Fig. 4. The results, in the same format as Fig. 4, are shown in Fig. 5.

The case A $h_{crit}^{\perp\,(A)}$ theoretical butterfly curve is shown in the lower part of Fig. 5. In this case, the need to obtain *minimum* threshold, and the effect of the $\Delta H_k(\mathbf{k})$ function in Eq. (24) on this minimum threshold, leads to the same basic kink effect obtained in the IP configuration. The actual threshold microwave field amplitudes, however, are *higher* by the factor of $\pi/2$ because of the nonzero $k_\perp$ condition for the PI configuration discussed in Sec. III. Note that the case A $h_{crit}^{\perp\,(A)}$ theoretical values are larger than the corresponding theoretical values on the case A $h_{crit}^{\parallel\,(A)}$ solid curve in Fig. 4 by about this factor. Note also that the case A $h_{crit}^{\perp\,(A)}$ curve is *above* the h_{crit} data in Fig. 5, except for the extreme high field portion of the butterfly curve. We see that the theory in this case gives a kink effect, but that the threshold fields are *higher* than the measured thresholds.

Turn now to the case B $h_{crit}^{\perp\,(B)}$ threshold curve in the lower part of Fig. 5. This curve was obtained on the basis of Eq. (23) in Sec. III, the *same* $\Delta H_k(\mathbf{k})$ function from Eq. (24) used for the other theoretical curves, the *same* ΔH_k parameters cited above, and the applicable PI case B dispersion constraint from the $\partial\omega_k/\partial k_\perp = 0$ condition as specified by Eq. (22). This curve matches the PI configuration data almost perfectly.

Recall that for the case B $h_{crit}^{\perp\,(B)}$ butterfly curve, there is no minimization procedure with respect to available (k, θ_k, $\omega_k = \omega_p/2$) modes as in the two previous cases just considered. The $\partial\omega_k/\partial k_\perp = 0$ dispersion constraint given in explicit form in Eq. (22), in combination with the dispersion relation in Eq. (12) for $\omega_k = \omega_p/2$ spin waves, *completely* specifies the case B $h_{crit}^{\perp\,(B)}$ critical mode k and θ_k values. For case B, therefore, we have a smooth variation in the critical mode k and θ_k values with static field and *no* kink effect. It is remarkable that one can use the *same* $\Delta H_k(\mathbf{k})$ trial function with the same numerical parameters for both the IP and the PI configurations, and obtain near perfect fits in both cases, one with and one without the kink effect. The diagram in the upper part of Fig. 5 shows the variations in the critical mode wave number k and the spin wave angle θ_k with static field associated with the case B $h_{crit}^{\perp\,(B)}$ butterfly curve in the lower part of the figure. Both k and θ_k simply decrease monotonically as the field increases. There are no jumps in the critical mode k or θ_k values with field, and there are no butterfly curve kinks.

We close this discussion by considering the critical mode k and θ_k behaviors associated with the kink effect and the "no kink" effect just discussed from a somewhat different perspective. Figure 6 shows a standard schematic spin wave manifold picture of the spin wave frequency ω_k as a function of wave number k for fixed static field. The upper and lower band limit curves correspond to θ_k propagation angles of 90° and 0° in the usual manner. The line of discontinuous slope in the diagram denotes the "trajectory" for the (k,θ_k) critical mode for a butterfly curve with the kink effect. At high k values, the critical mode follows a "trajectory" at $\theta_k \approx 35°$. When k decreases sufficiently, such that modes at $k \approx 0$ become available for θ_k values

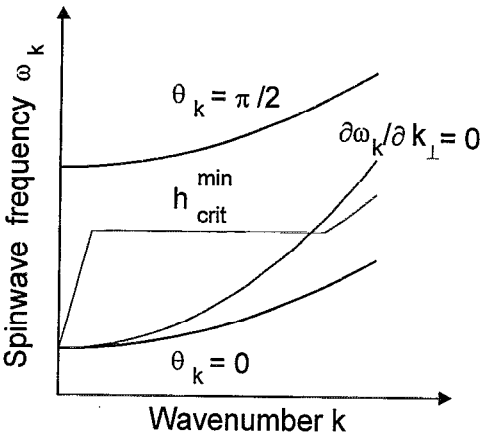

FIG. 6. Spin wave manifold diagram of spin wave frequency ω_k vs wave number k, with upper and lower band limit curves at θ_k propagation angles of $\pi/2$ (90°) and 0 in the usual manner. The smooth curve labeled as "$\partial\omega_k/\partial k_\perp = 0$" denotes the critical mode (k,θ_k) "trajectory" for butterfly curves with no kink effect, as for the data and case B curve in Fig. 5. The curve with the horizontal jump labeled "h_{crit}^{min}" denotes the (k,θ_k) "trajectory" for butterfly curves with the kink effect, as for the data and case A curve in Fig. 5.

somewhat below 90°, the minimum threshold critical mode "jumps" to $k \approx 0$ to reduce ΔH_k through the step function effect in Eq. (24). After this "jump" k stays at zero and θ_k decreases to zero. This trajectory maps the k and θ_k variations shown in Fig. 4 versus field. Keep in mind that in the actual fixed frequency experiment, the spin wave frequency is fixed, the static field is increasing, and the spin wave band is moving *up* in frequency. The dot-dash line "trajectory" in Fig. 6 is intended simply to map the (k,θ_k) behavior of the critical mode.

Turn now to the smooth line trajectory in Fig. 6. This line shows, in schematic form, the ω_k vs k variation which results from combining the spin wave dispersion equation of Eq. (12) and the additional constraint specified by Eq. (22). This trajectory is quite different from the dot-dash trajectory for the kink effect. In the IP configuration, the "kink" trajectory represents the minimum threshold critical mode and this trajectory yields the fitted butterfly curve shown in Fig. 4 and discussed above. In the PI configuration, the threshold microwave field amplitudes associated with the kink trajectory are *increased* by the $\pi/2$ factor discussed above. As a result, the lowest threshold is obtained with the dashed line "no kink" trajectory. This threshold corresponds to the theoretical butterfly curve indicated by the solid line in Fig. 5.

V. SUMMARY AND CONCLUSION

The above discussion has presented (1) experimental data on subsidiary absorption spin wave instability threshold microwave fields and related butterfly curves for single crystal films of yttrium iron garnet (YIG), (2) a summary of a theory for first order spin wave instability processes in thin films, and (3) theoretical analysis and fits of operational threshold microwave field equations to the data.

The data were obtained at 10 GHz and room temperature for two field configurations, one with the static field in plane and the microwave field out of plane and the other for the static field out of plane and the microwave field in plane. For the first case, the IP configuration, one obtains a butterfly curve with a characteristic kink, similar to previously reported results for YIG spheres and in plane magnetized films. For the second case, the PI configuration, one obtains a smooth butterfly curve with no kink.

The theory, published separately, extends previous work to the specific case of thin magnetic films. Operational equations are developed for two limiting cases and the specific IP and PI configurations used in the measurements. The two limiting cases are (A) the thin film limit in which the mode spacing in frequency is much greater than the YIG spin wave relaxation frequency, and (B) a limit applicable to thick films or special modes for which the mode spacing is much less than YIG relaxation frequency.

Fits to the data were based on a previously developed operational equation for the k-dependent spin wave linewidth $\Delta H_k(\mathbf{k})$ which lead to a quantitative explanation for the kink effect in spheres *and* critical mode predictions which have been verified by light scattering measurements. The *same* linewidth equation with the *same* parameters could be used to successfully fit the theory to the data for *both* the IP and the PI configurations. The fits were able to reproduce the kink effect butterfly curve for the IP configuration and the smooth kink free butterfly curve for the PI configuration. The analysis of the critical modes associated with the fits revealed very different properties in the two cases. In the "kink" case, the critical modes show jumps in wave number and propagation angle consistent with the previous work. In the "no kink" case, the wave number and propagation angle for the critical modes vary smoothly with field. These modes do not correspond to the minimum threshold critical modes expected from the bulk theory. Rather, they correspond to the modes needed to satisfy the B-limit mode spacing condition in the theory.

ACKNOWLEDGMENTS

Dr. G. Wiese was supported in part on a postdoctoral fellowship from the Deutsche Forschungsgemeinschaft, Bonn, Germany. The YIG films used in this work were kindly provided by Dr. J. D. Adam, Westinghouse Research Laboratories, Pittsburgh, Pennsylvania and Dr. P. DeGasperis, CNR, Rome, Italy. The research was supported in part by the United States Office of Naval Research, Grant No. N00014-90-J-4078, the National Science Foundation, Grant No. DMR-8921761, and the United States Army Research Office, Grant No. DAAL03-91-0327.

[1] H. Suhl, J. Phys. Chem. Solids **1**, 209 (1957).
[2] C. E. Patton and W. Jantz, J. Appl. Phys. **50**, 7082 (1979).
[3] W. D. Wilber, J. G. Booth, C. E. Patton, G. Shrinivasan, and R. W. Cross, J. Appl. Phys. **64**, 5477 (1988).
[4] C. E. Patton, J. Appl. Phys. **40**, 2837 (1969).
[5] M. Chen and C. E. Patton, J. Appl. Phys. **69**, 5724 (1991).
[6] G. Wiese, Z. Phys. B **82**, 453 (1989).
[7] G. Wiese, Z. Phys. B **91**, 57 (1993).
[8] E. Schlömann, Ferromagnetic Resonance at High Power Levels, Technical Report R-48, Raytheon Company, Research Division, October 1, 1959.
[9] C. E. Patton and W. Jantz, IEEE Trans. Magn. **14**, 698 (1978).
[10] C. E. Patton, Phys. Status Solidi B **92**, 211 (1979); B **93**, 63 (1979).
[11] S. M. Rezende and A. Azevedo, Phys. Rev. B **45**, 387 (1992).
[12] M. Sparks, *Ferromagnetic Relaxation Theory* (McGraw-Hill, New York, 1964).
[13] M. Chen and C. E. Patton, "Spin Wave Instability Processes in Ferrites," in *Nonlinear Phenomena and Chaos in Magnetic Materials*, edited by P. E. Wigen (World Scientific, Singapore, 1993).